Accepted Manuscript

Supercritical solvothermal synthesis and formation mechanism of V_2O_3 microspheres with excellent catalytic activity on the thermal decomposition of ammonium perchlorate

Liuqing Yang, Xiaofang Li, Xiongzhi Zhang, Chi Huang

PII: S0925-8388(19)32580-0

DOI: https://doi.org/10.1016/j.jallcom.2019.07.083

Reference: JALCOM 51371

To appear in: *Journal of Alloys and Compounds*

Received Date: 24 April 2019

Revised Date: 7 July 2019

Accepted Date: 8 July 2019

Please cite this article as: L. Yang, X. Li, X. Zhang, C. Huang, Supercritical solvothermal synthesis and formation mechanism of V_2O_3 microspheres with excellent catalytic activity on the thermal decomposition of ammonium perchlorate, *Journal of Alloys and Compounds* (2019), doi: https://doi.org/10.1016/j.jallcom.2019.07.083.

V_2O_3 with the structure of microsphere has been successfully synthesized by a facile supercritical solvothermal method. The as-obtained V_2O_3 microspheres had excellent catalytic activity on the thermal decomposition of AP.

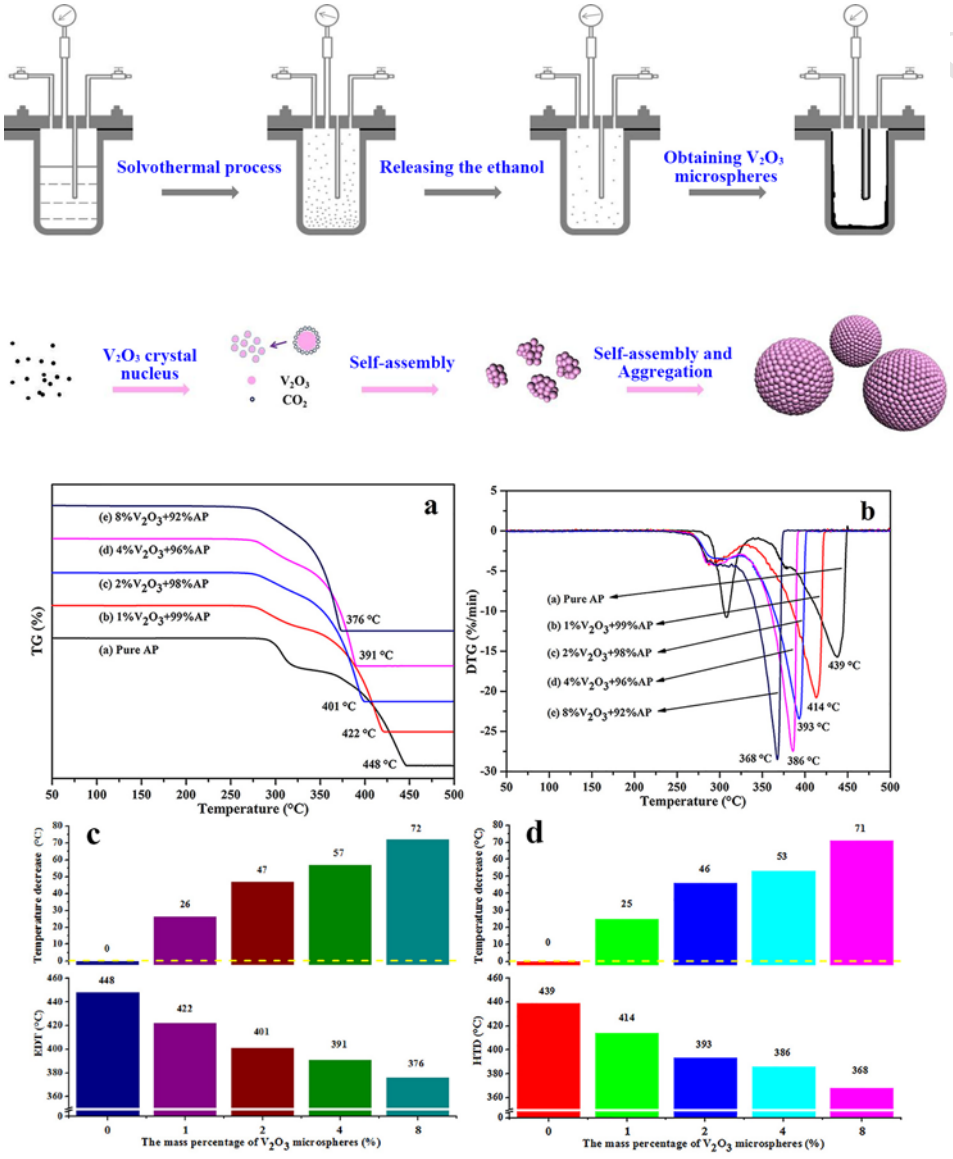

Supercritical Solvothermal Synthesis and Formation Mechanism of V_2O_3 Microspheres with Excellent Catalytic Activity on the Thermal Decomposition of Ammonium Perchlorate

Liuqing Yang [a, c], Xiaofang Li [b], Xiongzhi Zhang [b], Chi Huang [c*]

[a] Office of Educational Administration, Changzhi University, Changzhi 046011, PR China

[b] School of Chemistry and Chemical Engineering, Wuhan University of Science and Technology, Wuhan 430081, PR China

[c] College of Chemistry and Molecular Sciences, Wuhan University, Wuhan 430072, PR China

***Corresponding author:** Prof. C. Huang (chihuang@whu.edu.cn)

Abstract: V_2O_3 with the structure of microspheres has been successfully synthesized by a facile supercritical solvothermal method. The samples have a rhombohedral structure and the morphology of microspheres. The formation mechanism is proposed on the basis of the discussion on the self-assembly process of uniform microsphere structure. Furthermore, the catalytic activity of as-obtained V_2O_3 microspheres was investigated through the thermal decomposition of ammonium perchlorate (AP). The thermal decomposition temperature was reduced by 46 °C in the presence of 2 wt% of V_2O_3 microspheres, indicating that V_2O_3 with microspheres structure has excellent catalytic property. In addition, the possible catalytic mechanism of the microspheres for the thermal decomposition of AP is simply discussed. This study provides a simple way to control the morphology of V_2O_3 nanostructure, which also exhibits the potential application in modern science and technology.

Key words: *V_2O_3 microspheres; Supercritical solvothermal synthesis; Ammonium perchlorate; Catalytic activity*

1 Introduction

In the past decades, vanadium oxides with versatile structures, outstanding physical and chemical properties have drawn tremendous attention in science and were applied in the field of catalysts, electrical and optical devices, smart thermochromic coatings, lithium-ion batteries and so on [1-10]. In general, due to the extensive oxidation states of vanadium from 0 to + 5, a large number of oxides are usually conform to the common formula VO_{2+x} ($-0.5 \leq x \leq 0.5$), such as V_2O_3, VO_2, V_3O_7, V_2O_5 [11]. Among these oxides, vanadium sesquioxide (V_2O_3) has acquired great investigation as a multifunctional material owing to its high melting point, low thermal expansion, open tunnel structure, high theoretical capacity and metal-to-insulator phase transition, *etc* [12-14]. Furthermore, V_2O_3 has received various applications especially in catalysts.

Various strategies have been employed to control the morphologies of V_2O_3, including hydro/solvothermal method, pyrolysis, sol-gel, magnetron sputter and chemical vapor deposition [15-20]. Supercritical solvothermal process, as an easy method with many merits including moderate condition, reductive atmosphere, high reactant diffusivity and high supersaturation degree, can generate uniform particles with good crystallinity [21]. However, the synthesis and design of V_2O_3 with novel and special morphology using supercritical solvothermal process have been correspondingly rarely reported. Liu *et al*. [22] synthesized V_2O_3 nanoparticles with diameters of 30-60 nm by supercritical ethanol fluid reduction of VOC_2O_4. Balakhonov *et al*. [23] reported that vanadium oxide aerogels containing V_2O_3 were prepared by means of a supercritical drying technique putting mixtures of acetone and ethanol as supercritical solvents. Li *et al*. [24] found that sphere-like V_2O_3 with average particle sizes

of 20-50 nm was synthesized successfully in supercritical methanol using the inorganic metal salt as precursor directly. From the above literatures, although it is noted that nanosized V_2O_3 or the material containing V_2O_3 has been synthesized under supercritical conditions, macro-scale V_2O_3, especially microsphere which can be applied widely in energy storage fields, devices, catalysts and sensors due to its fascinating electrical and optical properties [25], low toxicity [26], increased surface area [27], has not been reported.

Herein, this work has investigated the fabrication of V_2O_3 microspheres via a facile supercritical solvothermal process by the reduction of VOC_2O_4 precursor in ethanol. In the process of the reaction, supercritical ethanol played a role of a reducing agent. The presence of CO_2 served as surface stabilizer to establish morphology and the V_2O_3 microspheres were assembled with nanoparticles as the primary building blocks. Besides, the formation mechanism of the microsphere was proposed. Finally, the as-obtained V_2O_3 microspheres were introduced to catalyze the thermal decomposition of ammonium perchlorate (AP), which is the most common oxidizer used in solid propellants.

2 Experimental

2.1 Synthesis of V_2O_3 microspheres

All of the reagents with analytical grade were purchased from Sinopharm Chemical Reagent Co., Ltd. and used directly without any further purification. In a modified procedure refer to previous paper [22], 0.8 g of V_2O_5 and 1.5 g of $H_2C_2O_4 \cdot 2H_2O$ were dispersed into 50 mL of ethanol and the mixture was added to a 100 mL two-necked flask, followed by refluxing at 80 °C for about 3 h to obtain an emerald solution. It should be known that if some precipitation was observed in the green solution, the process of filtration must be carried out.

Subsequently, 40 mL of the above solution was transferred into a 60 mL stainless steel autoclave with a needle-like valve to release the internal fluid, which was sealed and heated to get supercritical ethanol conditions (250 °C and 7.5 MPa). After the autoclave was maintained for 4 h under supercritical conditions, the ethanol was released from the needle-like valve under different time (2 h, 4 h, 6 h and 8 h). Then the autoclave was cooled to room temperature naturally to obtain the black powder. The as-obtained products were washed with distilled water and absolute ethanol several times to remove any possible residue and dried at 70 °C in a vacuum oven.

2.2 Characterization

The structure of the powder was investigated by X-ray powder diffraction (XRD, Bruker D8-Advance X-ray diffractometer, Cu *K*α radiation, λ = 1.54056 Å) between 10° and 80° with a scan speed of 6°/min. The morphology of the product was observed by scanning electron microscopy (SEM, Quanta 200, 30 kV) and transmission electron microscopy (TEM, JEM-2100). Fourier transform infrared spectroscopy (FT-IR) pattern of the sample was measured using KBr pellet technique and recorded on a Nicolet 60-SXB spectrometer from 4000 to 400 cm^{-1} with a resolution of 4 cm^{-1}. The chemical composition of the as-obtained sample was analyzed by using the energy dispersive X-ray spectrometer (EDS, Quanta 200). The phase transition temperature (Tc) of the sample was tested by DSC (DSC822e, METTLER TOLEDO) with the heating rate of 5 K/min. The catalytic property of the V_2O_3 product was performed by thermo-gravimetric analysis (TG 209 F1 Libra®, NETZSCH) at a heating rate of 10 K/min in N_2 atmosphere in the range of 25-500 °C and the mass percentages were 1, 2, 4 and 8 %, respectively.

3 Results and discussion

3.1 Characterization of structure and morphology

The crystallization and structural information of the as-abtained samples after solvothermal treatment under supercritical conditions were studied by using the X-ray diffraction. The XRD patterns are shown in Fig.1. All of diffraction peaks can be indexed to a rhombohedral structure of V_2O_3 (JCPDS, No. 84-0317) with space group R-3c and lattice parameters of a = 4.9322 Å, b = 4.9323 Å, and c = 13.9910 Å [28]. No characteristic peaks of any other phases or impurities are observed, which suggests the synthesis of pure V_2O_3 phase. The peaks belonging to the (11*l*) serials indicate that the V_2O_3 nanoparticles have a preferential growth direction.

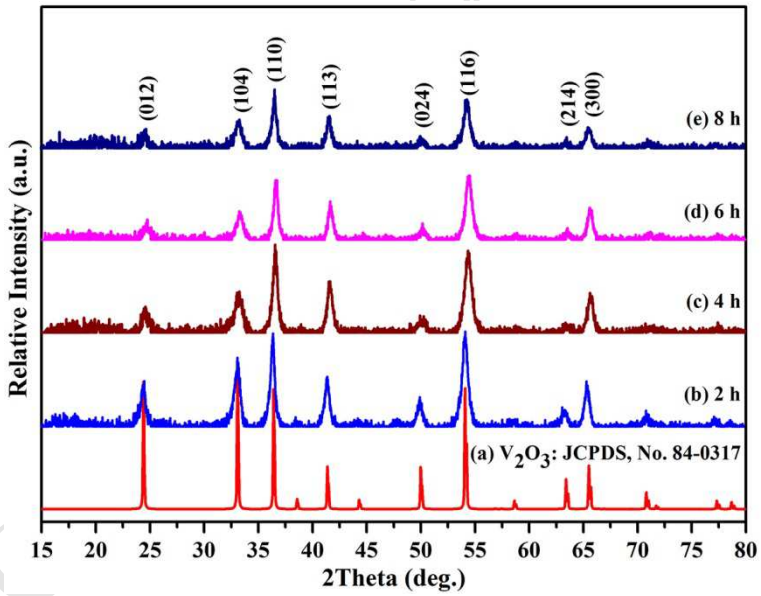

Fig. 1 XRD patterns of the as-obtained V_2O_3 microspheres

The average crystallite sizes of the V_2O_3 samples were calculated on the basis of the broadening of the (110) diffraction peak by Debye-Scherer formula [29]:

$$D = \frac{K\lambda}{\beta \cos\theta}$$

where D is the average crystallite size, *K* denotes the Scherer constant (the shape factor of the

average crystallite and is equal to 0.89), λ is the X-ray wave length of Cu K_α radiation (1.54056 Å), β is the full width at half maximum (FWHM) of the selected peak and θ is the Braggs diffraction angle in degrees. The calculated values of average crystallite size for the samples are summarized in Table 1. It is revealed from the results that there is a variation in the crystallite size of the as-obtained V_2O_3 microspheres from 35.0 nm to 16.8 nm when the time of the ethanol released from the needle-like valve varies from 2 h to 8 h.

The above equation gives the information about average crystallite size of the crystal only, however, the another fact of XRD signature is the broadening of peaks. And the broadening of X-ray peaks is related not only to crystallite size or change in lattice structure but also to the role of lattice strain (ε) that arises from imperfect and distorted crystals during the synthesis process. The lattice strain can be estimated according to the Stokes-Wilson equation [30]:

$$\varepsilon = \frac{\beta}{4\tan\theta}$$

where ε is lattice strain, β is the FWHM of the peak and θ is Braggs angle. The results are shown in Table 1 and it is obvious to be seen that the average crystallite size decreases while lattice strain increases with the time of the ethanol released from the needle-like valve. Besides, it can be seen that all of the peak widths are broaden, which is attributed to the small particle size.

Table 1 Important parameters of the as-obtained V_2O_3 microspheres from XRD and SEM

Samples	XRD				SEM
	FWHM (°)	2θ (°)	Crystallite size D_{XRD} (nm)	Lattice strain ε (10^{-3})	Microsphere size D_{SEM} (nm)
2 h	0.2364	36.4508	35.0	3.1	1352
4 h	0.3941	36.6084	21.0	5.2	863
6 h	0.4730	36.6281	17.5	6.2	750
8 h	0.4926	36.6478	16.8	6.5	646

The morphology and microstructure of the typical V_2O_3 samples were observed by using SEM and TEM. The sample under the release time of 2 h for the ethanol is composed of a large number of microspheres with the diameter distribution ranging from 1.2 μm to 1.5 μm and an average diameter of around 1.4 μm, which can be clearly seen from an overall view in Fig. 2a. The magnified images of single microsphere presented in Fig. 2b, c reveal that the surface is rough and composed of numerous nanoparticles with the size distribution ranging from 137 nm to 220 nm and an average size of around 175 nm as resulting in full of sags and crests. The rough surface of the microspheres is likely to indicate that the microspheres were aggregated and self-assembled by nanoparticles under the supercritical conditions and the process of the ethanol released from the needle-like valve. The microsphere morphology of the V_2O_3 could further be demonstrated by its TEM images shown in Fig. 2d-f. As seen in Fig. 2d, the synthesized sample exhibits relatively homogeneous size. The roughness of V_2O_3 microspheres surface is more evident and the inner is packed loosely, which could be seen clearly in Fig.2e. And in the high magnification image (Fig. 2f), the nanoparticles could be obviously observed that the size distribution ranged from 127 nm to 210 nm and the average

particle size was 174 nm, corresponding to the result of SEM image.

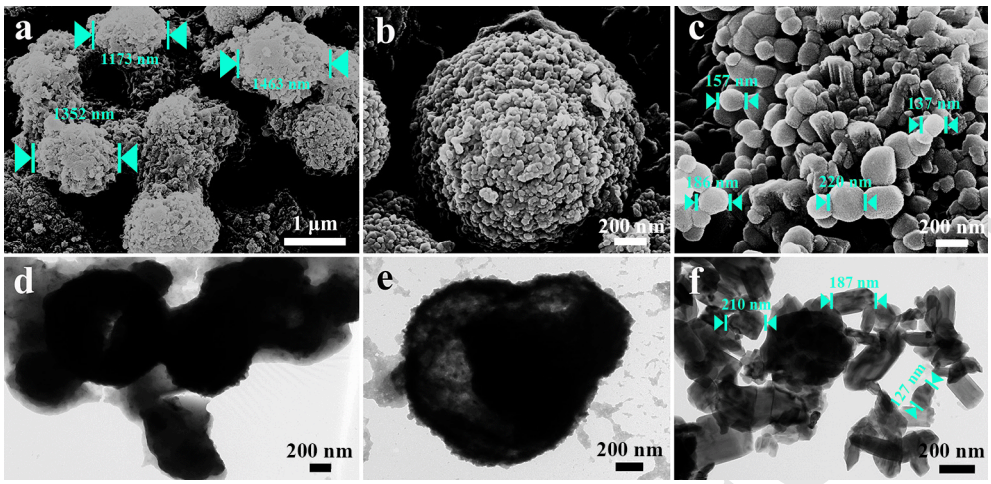

Fig. 2 SEM images (a-c) and TEM images (d-f) of the as-obtained V_2O_3 microspheres under the release time of 2 h for the ethanol

Further investigations were carried out by SEM and TEM to provide detailed insights into the microstructure change of the samples under the release time of 4 h, 6 h and 8 h for the ethanol. The all synthesized samples diplay homogeneous microsphere morphology, whereas some differences in size and inner part could be observed from these images. Fig. 3a shows microspheres with an average size of about 863 nm when the ethanol was released from the needle-like valve under the time of 4 h. The looser structure, rough surface and pale inner part are exhibited from the individual microsphere through the high-magnitude SEM and TEM images in Fig. 3b and c. Upon increasing the release time for the ethonal, it can be seen that the size of V_2O_3 samples has an appreciable variation from 750 nm to 646 nm under the time of 6 h and 8 h. And it also could be obviously observed that the single microsphere surface becomes more and more tight and the inner part shows more solid, especially under the time of 8 h, which probably results from the influence of the pressure and the time to the grain growth under the process that the ethanol was released from the needle-like valve. The all

values of microspheres size calculated from SEM images are summarized in Table 1. It is noteworthy to mention that the variation trend of the microsphere size calculated from SEM images is consistent with the crystallite size estimated via XRD. The truth is that the microsphere was formed on account of the aggregation and growth of small crystals in the solvothermal synthesis under the supercritical conditions. The detailed formation mechanism would be proposed in the following section.

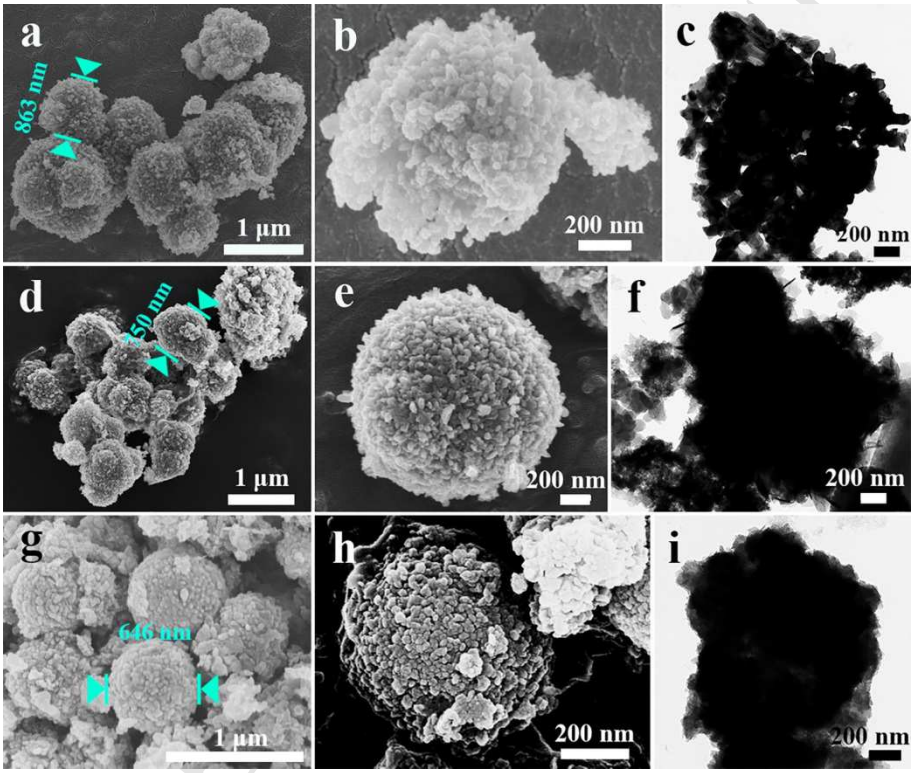

Fig. 3 SEM and TEM images of the as-obtained V_2O_3 microspheres under the release time of 4 h (a-c), 6 h (d-f) and 8 h (g-i) for the ethanol

To further confirm the composition of the obtained materials, the corresponding characterizations, that FT-IR and EDS, were also carried out. The FT-IR spectra in the wavelength region of 4000-400 cm^{-1} for the V_2O_3 samples are shown in Fig. 4a, from which the structure information and chemical bonding between vanadium and oxygen ions can be more acquired. The analysis of the spectra shows the existence of bands relating to the

vanadium-oxygen stretching vibrations between 400 and 1000 cm^{-1}. The peak at 987 cm^{-1} corresponds to the symmetric stretching vibration of the $\nu(V^{3+}=O)$ bond [31-33]. Meanwhile, the weak peak at 847 and the strong peak at 562 cm^{-1} can be attributed to the asymmertic and symmetric stretching vibrations of the ν(V-O-V) bridging bonds [34, 35]. There is not change for the position of characteristic bonds but the intensity with the increase of the time, which can be ascribed to the detectable presence of organic substances observed from other peaks in the spectra. The result from sample annealed in argon (99.999 %) atmosphere at 600 °C for 3 h confirrms the truth further. Besides, the peaks that can be negligible are seen at 3404 cm^{-1} and 1637 cm^{-1} respectively, originating from the O-H stretching vibration and bending vibration of water adsorbed on the surface of the crystallites or KBr [36]. Some characteristic groups including C-H, C=O that could also be neglected are obviously observed in the FT-IR spectra. The peaks at around 2926 cm^{-1} and 1407 cm^{-1} are the characteristic C-H stretch and bend, suggesting the existence of residual C-H groups. The peak at 2364 cm^{-1} is attributed to O=C=O vibrations from CO_2. The C-H groups and CO_2 are assigned to molecules absorbed on the microspheres or in atmosphere so that which still remains in the spectrum after annealing treatment. The EDS spectrum of V_2O_3 microspheres for 2 h is displayed in Fig. 4b, which reveals that the surface of the sample is only composed of V and O elements and no other contaminants are detected. The conformed structure of V_2O_3 phase is consistent with the data obtained from XRD. Based on the above analyses, V_2O_3 micrpspheres were successfully synthesized.

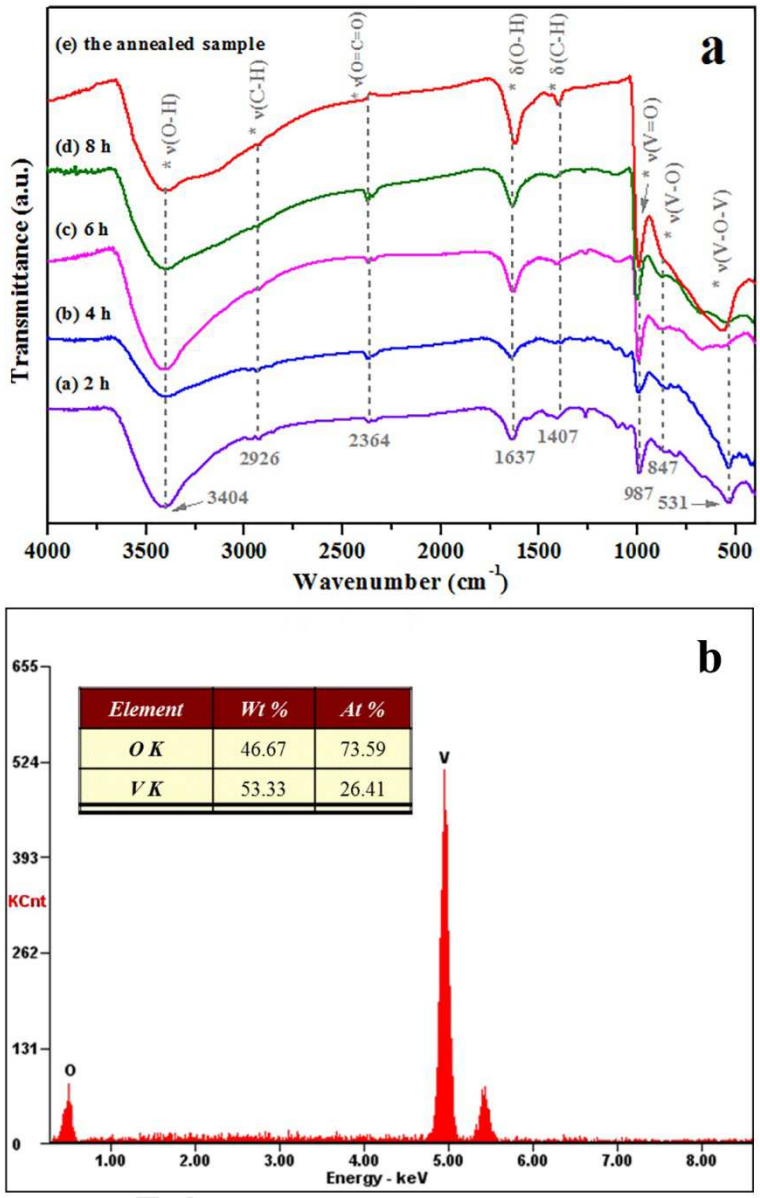

Fig. 4 FT-IR (a) and EDS (b) spectra of the as-obtained V_2O_3 microspheres

Lots of intense researches were carried out on V_2O_3 due to a temperature-induced reversible metal-to-insulator transition (MIT) between rhombohedral phase (R-3c) and monoclinic phase (I2/a) [15, 37-40]. The phase transition behavior of the microspheres with the release time of 2 h was investigated using DSC which can record a noticeable endothermal and exothermal profile in its heating and cooling curves. In this work, the typical DSC curves of V_2O_3 microspheres in the heating and cooling cycles are shown in Fig. 5. The phase transition temperature (T_c) of V_2O_3 is about -110.3 °C according to an endothermic

peak upon the heating curve (Fig. 5a) and about -131.2 °C according to an exothermic peak upon the cooling curve (Fig. 5b) , with a temperature hysteresis width of 20.9 °C, accompanying the crystal structure change from monoclinic to rhombohedral and from rhombohedral to monoclinic respectively. The result corresponds to the first-order phase transition of V_2O_3 and is consistent with our previous reports [31, 41]. Meanwhile, it is observed that the phase transition of V_2O_3 has good reversibility during the cooling-heating circle.

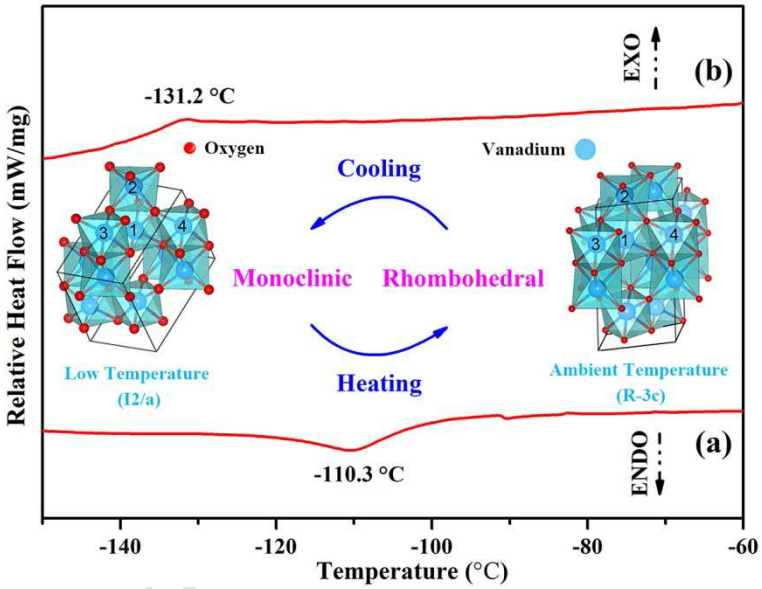

Fig. 5 DSC curves of the as-obtained V_2O_3 microspheres

3.2 Possible formation mechanism of V_2O_3 microspheres

Based on the above analysis, a possible formation mechanism of the V_2O_3 microspheres is illustrated in Fig. 6 in depth. And the basic reaction employed for this synthesis can be formulated by the following eq. (1) and eq. (2) [22]:

$$V_2O_5 + 3H_2C_2O_4 \rightarrow 2VOC_2O_4 + 2CO_2 + 3H_2O \quad (1)$$

$$2VOC_2O_4 + CH_3CH_2OH \rightarrow V_2O_3 + CH_3CHO + 2CO + 2CO_2 + H_2O \quad (2)$$

Firstly, vanadyl oxalate (VOC_2O_4) solution should be prepared by the reduction between

V_2O_5 and oxalic acid in ethanol solution with refluxing. Then, VO_2^+ dissociating from VOC_2O_4 was reduced to V_2O_3 crystal nucleus by the ethanol acting as the reducing reagent and supercritical ingredient under the solvothermal condition. The V_2O_3 primary nucleus was an initial ordered structure which was lucky enough to overcome the critical size and quickly grown to macroscopic dimensions on a time scale much smaller than the long time required for that fortunate fluctuation to come about. Meanwhile, the as-formed CO_2 played an important role to prevent V_2O_3 particles from aggregating together fastly and control the V_2O_3 morphology by surrounding the V_2O_3 crystal nucleus. It cannot be denied that larger V_2O_3 nanoparticles would be more or less formed at the cost of those crystal nucleus, according to the classic Ostwald ripening as the common crystal growth mechanism in solvothermal synthesis [42]. When the supercritical ethanol was released from needle-like valve of the autoclave during different times, the inner pressure of the autoclave would decrease and the CO_2 bubbles around the V_2O_3 crystal nucleus would also be eliminated simultaneously. In consequence, the dispersed V_2O_3 nanoparticles under high temperature condition would possess quite high surface energy owing to the above operation and tend to self-assembly process to decrease the surface energy by reducing the exposed areas. Lastly, V_2O_3 microspheres were eventually formed by the further aggregation of V_2O_3 nanoparticles with the continual depression of pressure in the autoclave resulting from the release of the internal fluid. However, there are some differences in the morphology of microspheres obtained by varying the release time of the ethanol, which has been proved by the SEM and TEM results. Many pores were yielded associating with the self-assembly of nanoparticles for the time of 2 h and 4 h due to fast aggregation of nanoparticles induced by the change of reaction condition.

And these pores were highly desirable for catalytic applications because they could provide larger surface area to contact with substance. With prolonged release time, the change of reaction condition was relatively slow so that smaller size microspheres were formed under a longer growth process which promoted V_2O_3 nanoparticles and fresh formed crystal nucleus to achieve sufficient self-assembly mechanism. This is the reason why V_2O_3 microspheres without pores but solid interior were obtained under the release time of 6 h and 8 h. In addition, the oriented attachment was also a significant formation mechanism of V_2O_3 microspheres by crystallographically controlled self-assembly of tinier crystals, which can be in accordance with XRD results that some diffraction peaks are pronounced [43].

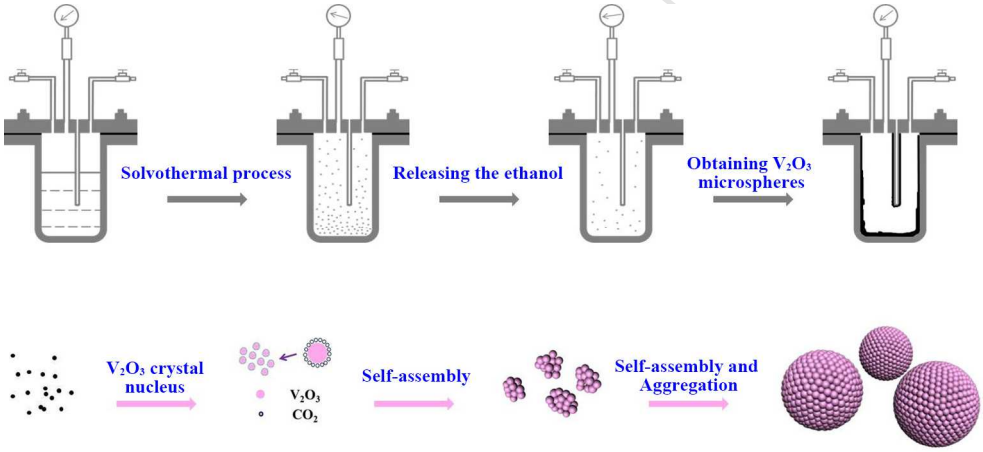

Fig. 6 Possible formation mechanism of V_2O_3 microspheres

3.3 Catalytic activity and mechanism of V_2O_3 microspheres

As a widely used oxidizer in solid propellants, the thermal decomposition process of AP will strongly affect on the combustion behavior of the solid propellant directly and further on the performance of the aerospace vehicles [44-46]. It is one of significant researches for improving the thermal decomposition performance of AP by using the catalyst to promote the decomposition and reduce the decomposition temperature of AP. Therefore, the catalytic effect of the as-obtained V_2O_3 microspheres with the release time of 2 h on the thermal

decomposition of AP was explored by the TG/DTG experiment. TG and DTG curves of pure AP and AP in the presence of V_2O_3 microspheres (1, 2, 4 and 8 wt%) are shown in Fig.7. It is obvious according to the figures that V_2O_3 microspheres accelerate the thermal decomposition of AP. The starting decomposition temperature of AP is decreased by the addition of V_2O_3, but the amount has little effect on it. With the addition of V_2O_3, it can be distinctly observed from Fig.7a and c that the ending decomposition temperatures (EDT) have a significant reduction from 448 °C of pure AP to 422, 401, 391 and 376 °C and decrease by 26, 47, 57 and 72 °C.

The corresponding DTG curves of AP and the mixtures with V_2O_3 are shown in Fig.7b and two peaks can be seen in each curve, which exhibits that the thermal decomposition of AP can be generally divided into two steps. The first decomposition step, namely the low temperature decomposition (LTD), is a solid-gas multiphase reaction including decomposition and sublimation procedures. During LTD step, a proton transfers from the cation NH_4^+ to the anion ClO_4^- to form NH_3(g) and $HClO_4$(g), which may be described as follows [47]:

$$NH_4ClO_4(s) \rightarrow NH_4^+ + ClO_4^- \rightarrow NH_3(s) + HClO_4(s) \rightarrow NH_3(g) + HClO_4(g)$$

The second decomposition step is high temperature decomposition (HTD), which is attributed to the reaction of the gas-phase products of AP. During HTD step, the $HClO_4$ could timely decompose to form O_2 and further generate the superoxide radical anion ($\cdot O_2^-$) with the electron transfer process. Then, the $\cdot O_2^-$ with power oxidation can reacted with NH_3 to form final products. The specific thermal decomposition process of AP is illustrated in Fig.8.

From the experimental results in Fig. 7b and d, the HTD step is greatly influenced and the decomposition temperature for AP with the addition of 1, 2, 4 and 8 wt% V_2O_3 as catalyst are 414, 393, 386 and 368 °C whereas pure AP at 439 °C. The results demonstrate a decrease

of 25, 46, 53 and 71°C for the thermal decomposition of AP, which indicates the excellent catalytic activity of V_2O_3 microspheres.

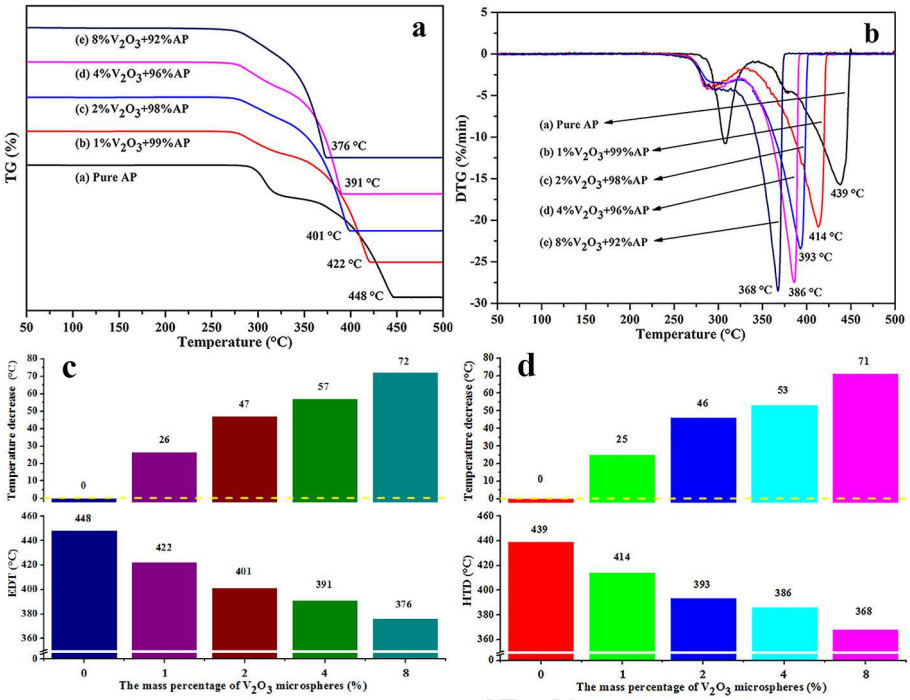

Fig. 7 TG (a) and DTG (b) curves of pure AP and AP with V_2O_3 microspheres, histogram of the corresponding ending decomposition temperatures and the temperatures decrease in Fig. 7a (c), histogram of the corresponding high temperature decomposition (HTD) and the temperatures decrease in Fig. 7b (d)

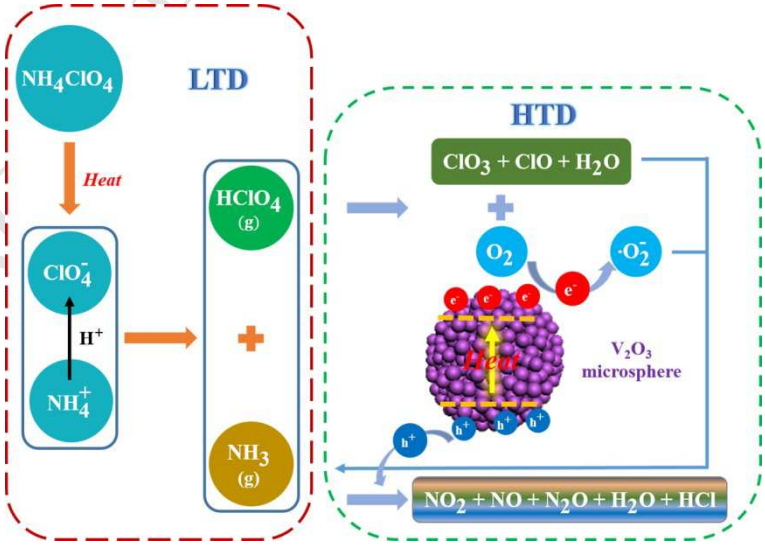

Fig. 8 Schematic illustration of the thermal decomposition process of AP with V_2O_3 microspheres

The catalytic performance of V_2O_3 microspheres in this work was also compared with that of V_2O_3 nanoparticles and other oxides microspheres in previous reports to display the relevance. As shown in Table 2, the V_2O_3 microspheres in this study could catalyze AP decomposition at lower temperature, compared with V_2O_3 nanoparticles and Ni-P alloy microspheres. To be noted, it was not lowest in terms of the decrease of EDT and HTD of AP. However, such factors as the synthesis methods of microspheres and catalytic mechanism, were considered appropriately, the catalytic property of V_2O_3 nanoparticles was excellent.

Table 2 The comparison of catalytic activity for ammonium perchlorate of different type of V_2O_3 and various oxides microspheres

Materials	Mass %	EDT (°C)		Decrease of EDT (°C)	HTD (°C)		Decrease of HTD (°C)	Ref.
		Pure AP	AP + Sample		Pure AP	AP + Sample		
V_2O_3 nanoparticles	2	460	415	45	-	-	-	[48]
Fe_3O_4 microspheres	2	463	383	80	455	397	58	[44]
Co_3O_4 microspheres	2	463	389	74	455	382	73	[44]
CuO microspheres	2	413	348	65	-	-	-	[49]
Ni-P alloy microspheres	2.17	443	397	46	-	-	-	[50]
V_2O_3 microspheres	2	448	401	47	439	393	46	This work

Based on the above results, the thermal decomposition of AP is mainly accelerated during the high temperature decomposition process by the V_2O_3 microspheres, because the corresponding decomposition temperature is dramaticlly reduced. In terms of the results, the possible catalytic mechanism of the as-obtained V_2O_3 microspheres may be ascribed to the novel structure, which could produce more active sites to promote the decomposition. Above all, it is beneficial to absorb the gas molecular generated in the primary thermal

decomposition process of AP on their surface. Furthermore, the partially filled 3d orbit in V atom provides help in the electro-transfer process according to the traditional electron-transfer theory [51, 52]. Meanwhile, the positive hole (h^+) in V atom can accept electrons from intermediate products of AP, by which the thermal decomposition of AP is further accelerated.

4 Conclusions

In summary, V_2O_3 with the structure of microspheres has been successfully synthesized by a facile supercritical solvothermal method using VOC_2O_4 as precursor directly prepared via commercial V_2O_5 and $H_2C_2O_4 \cdot 2H_2O$ as the starting materials. The samples have a rhombohedral structure and the morphology of microspheres. The formation mechanism is proposed on the basis of the discussion on the self-assembly process of uniform microsphere structure. To explore the potential application of the product, the catalytic effect of V_2O_3 microspheres on the thermal decomposition performance of AP was investigated. The thermal decomposition temperature was reduced by 46 ℃ in the presence of 2 wt% V_2O_3 microspheres, indicating that the as-obtained V_2O_3 microspheres have excellent catalytic property. The possible catalytic mechanism of the V_2O_3 microspheres for the thermal decomposition of AP is simply discussed.

Acknowledgements

This work was financially supported by the National Nature Science Foundation of China (No. 51572201).

References

[1] L.M. Zhang, F. Xia, Z.D. Song, N.A.S. Webster, H.J. Luo, Y.F. Gao, Synthesis and formation mechanism of VO_2(A) nanoplates with intrinsic peroxidase-like activity, RSC Adv. 5 (2015) 61371-61379.

[2] Y. Wang, G.Z. Cao, Synthesis and enhanced intercalation properties of nanostructured vanadium oxides, Chem. Mat. 18 (2006) 2787-2804.

[3] S. Beke, A review of the growth of V_2O_5 films from 1885 to 2010, Thin Solid Films 519 (2011) 1761-1771.

[4] B.M. Weckhuysen, D.E. Keller, Chemistry, spectroscopy and the role of supported vanadium oxides in heterogeneous catalysis, Catal. Today 78 (2003) 25-46.

[5] S.F. Wang, M.S. Liu, L.B. Kong, Y. Long, X.C. Jiang, A.B. Yu, Recent progress in VO_2 smart coatings: Strategies to improve the thermochromic properties, Prog. Mater. Sci. 81 (2016) 1-54.

[6] H. Zhang, X.D. Xiao, X.M. Lu, G.Q. Chai, Y.M. Sun, Y.J. Zhan, G. Xu, A cost-effective method to fabricate VO_2 (M) nanoparticles and films with excellent thermochromic properties, J. Alloy. Compd. 636 (2015) 106-112.

[7] Y.D. Zhang, Y. Li, X.H. Xia, X.L. Wang, C.D. Gu, J.P. Tu, High-energy cathode materials for Li-ion batteries: A review of recent developments, Sci. China-Technol. Sci. 58 (2015) 1809-1828.

[8] Y.F. Gao, H.J. Luo, Z.T. Zhang, L.T. Kang, Z. Chen, J. Du, M. Kanehira, C.X. Cao, Nanoceramic VO_2 thermochromic smart glass: A review on progress in solution processing, Nano Energy 1 (2012) 221-246.

[9] D.L. da Silva, E.C. Moreira, F.T. Dias, V.D. Neves Vieira, I.S. Brandt, A.D. Cas Viegas, A.A. Pasa, Quasi-one-dimensional nanostructured cobalt (Co) intercalated vanadium oxide (V_2O_5): Peroxovanadate sol gel synthesis and structural study, J. Solid State Chem. 221 (2015) 116-125.

[10] X.F. Li, L.Q. Yang, S.W. Zhang, X.J. Li, VO_2(M) with narrow hysteresis width from a new metastable phase of crystallized $VO_2(M)\cdot 0.25H_2O$, Mater. Lett. 211 (2018) 308-311.

[11] Y.F. Zhang, VO_2(B) conversion to VO_2(A) and VO_2(M) and their oxidation resistance and optical switching properties, Mater. Sci. 34 (2016).

[12] Y. Shi, Z.J. Zhang, D. Wexler, S.L. Chou, J. Gao, H.D. Abruña, H. Li, H. Liu, Y. Wu, J. Wang, Facile synthesis of porous V_2O_3/C composites as lithium storage material with enhanced capacity and good rate capability, J. Power Sources 275 (2015) 392-398.

[13] L. Jiang, Y. Qu, Z.Y. Ren, P. Yu, D.D. Zhao, W. Zhou, L. Wang, H.G. Fu, In situ carbon-coated yolk-shell V_2O_3 microspheres for lithium-ion batteries, ACS Appl. Mater. Interfaces 7 (2015) 1595-1601.

[14] H. Jiang, G.Q. Jia, Y.J. Hu, Q.L. Cheng, Y. Fu, C.Z. Li, Ultrafine V_2O_3 nanowire embedded in carbon hybrids with enhanced lithium storage capability, Ind. Eng. Chem. Res. 54 (2015) 2960-2965.

[15] Y.F. Sun, B.Y. Qu, S.S. Jiang, C.Z. Wu, B.C. Pan, Y. Xie, Highly depressed temperature-induced metal-insulator transition in synthetic monodisperse 10-nm V_2O_3 pseudocubes enclosed by {012} facets, Nanoscale 3 (2011) 2609-2614.

[16] Y. Xu, L. Zheng, C. Wu, F. Qi, Y. Xie, New-phased metastable V_2O_3 porous urchinlike micronanostructures: facile synthesis and application in aqueous lithium ion batteries, Chem.-Eur. J. 17 (2011) 384-391.

[17] Y.X. Guo, C.W. Zou, Y.F. Liu, Y.Q. Xu, X.L. Wang, J.Y. Yu, Z.Y. Yang, F. Zhang, R. Zhou, Facile preparation of vanadium oxide thin films on sapphire (0001) by sol–gel method, J. Sol-Gel Sci. Technol. 70 (2014) 40-46.

[18] Y. Shimazu, T. Okumura, A. Shimada, K. Tanabe, K. Tokiwa, E. Sakai, H. Kumigashira, T. Higuchi, Electronic structure of V_2O_3 thin film prepared by RF magnetron sputtering using oxygen radical and V-metal, Jpn. J. Appl. Phys. 53 (2014) 06JG05.

[19] G. Rampelberg, B. De Schutter, W. Devulder, K. Martens, I. Radu, C. Detavernier, In situ X-ray diffraction study of the controlled oxidation and reduction in the V–O system for the synthesis of VO_2 and V_2O_3 thin films, J. Mater. Chem. C 3 (2015) 11357-11365.

[20] D.M. Minic, V.A. Blagojevic, Hydrothermal synthesis and controlled growth of vanadium oxide nanocrystals, Crystengcomm 15 (2013) 6617-6624.

[21] N. Ye, T. Yan, Z. Jiang, W. Wu, T. Fang, A review: Conventional and supercritical hydro/solvothermal synthesis of ultrafine particles as cathode in lithium battery, Ceram. Int. 44 (2018) 4521-4537.

[22] X.H. Liu, Y.F. Zhang, S.P. Yi, C. Huang, J. Liao, H.B. Li, D. Xiao, H.Y. Tao, Preparation of V_2O_3 nanopowders by supercritical fluid reduction, J. Supercrit. Fluids 56 (2011) 194-200.

[23] S.V. Balakhonov, M.V. Efremova, V.K. Ivanov, B.R. Churagulov, Facile synthesis of vanadia aerogels with controlled $V^{3+}/V^{4}+$ ratio, Mater. Lett. 156 (2015) 109-112.

[24] S.M. Li, Z. Zhang, S.N. Jiang, X. Ge, J. Zhang, W.X. Li, S.S. Yu, Facile preparation and formation

mechanism of three low valent transition metal oxides in supercritical methanol, J. Mater. Res. 31 (2016) 1440-1447.

[25] Q. He, X.D. Xu, M. Wang, M.H. Sun, Y.D. Jiang, J. Yao, T.H. Ao, Chemical structures and physical properties of vanadium oxide films modified by single-walled carbon nanotubes, Phys. Chem. Chem. Phys.18 (2016) 1422-1428.

[26] R. Tang, X. Li, Z. Ding, L. Zhang, An ultrafine V_2O_3 modified hierarchical porous carbon microsphere as a high performance cathode matrix for lithium–sulfur batteries, RSC Adv. 6 (2016) 65162-65170.

[27] D. McNulty, D.N. Buckley, C. O'Dwyer, Comparative electrochemical charge storage properties of bulk and nanoscale vanadium oxide electrodes, J. Solid State Electrochem. 20 (2016) 1445-1458.

[28] L.W. Finger, R.M. Hazen, Crystal structure and isothermal compression of Fe_2O_3, Cr_2O_3, and V_2O_3 to 50 kbars, J. Appl. Phys. 51 (1980) 5362.

[29] A.J. Edwards, H.P. Klug, L.E. Alexander, x-ray diffraction procedures for polycrystalline and amorphous materials: Wiley-Interscience, New York, 1974, pp. 966

[30] A. R. Stokes, A.J.C. Wilson, The diffraction of X rays by distorted crystal aggregates - I, Proc. Phys. Soc. 56 (1944) 174-181.

[31] Y.F. Zhang, N.N. Wang, Y.T. Huang, C. Huang, X. Mei, C.G. Meng, Synthesis of V_2O_3/C composites with different morphologies by a facile route and phase transition properties of the compounds, Mater. Sci. 32 (2014) 236-242.

[32] I.L. Botto, M.B. Vassallo, E.J. Baran, G. Minelli, IR spectra of VO_2 and V_2O_3, Mater. Chem. Phys. 50 (1997) 267-270.

[33] Y.F. Zhang, Designed Synthesis and supercapacitor electrode of V_2O_3@C core-shell structured nanorods with excellent pseudo-capacitance in Na_2SO_4 neutral electrolyte, ChemistrySelect 3 (2018) 1577–1584.

[34] I. Mjejri, N. Etteyeb, F. Sediri, Vanadium oxides nanostructures: Hydrothermal synthesis and electrochemical properties, Mater. Res. Bull. 60 (2014) 97-104.

[35] L.J. Mao,C.Y. Liu, J. Li, Template-free synthesis of VO_x hierarchical hollow spheres, J. Mater. Chem. 18 (2008) 1640–1643.

[36] Y.F. Zhang, F.F. Zhang, L. Yu, M.J. Fan, Y.L. Zhong, X.H. Liu, Y.Y. Mao, C. Huang, Synthesis and characterization of belt-like VO_2(B)@carbon and V_2O_3@carbon core-shell structured composites,

Colloid Surf. A-Physicochem. Eng. Asp. 396 (2012) 144-152.

[37] F.J. Morin, Oxides which show a metal-to-insulator transition at the neel temperature, Phys. Rev. Lett. 3 (1959) 34-36.

[38] C. Meneghini, S. Di Matteo, C. Monesi, T. Neisius, L. Paolasini, S. Mobilio, C.R. Natoli, P.A. Metcalf, J.M. Honig, Antiferromagnetic-paramagnetic insulating transition in Cr-doped V_2O_3 investigated by EXAFS analysis, J. Phys. Condes. Matter 21 (2009) 355401.

[39] Y. Ding, C.C. Chen, Q. Zeng, H.S. Kim, M.J. Han, M. Balasubramanian, R. Gordon, F. Li, L. Bai, D. Popov, S.M. Heald, T. Gog, H.K. Mao, M. van Veenendaal, Novel high-pressure monoclinic metallic phase of V_2O_3, Phys. Rev. Lett.112 (2014) 056401.

[40] J. Trastoy, Y. Kalcheim, J. del Valle, I. Valmianski, I.K. Schuller, Enhanced metal-insulator transition in V_2O_3 by thermal quenching after growth, J. Mater. Sci. 53 (2018) 9131-9137.

[41] Y.F. Zhang, C. Huang, C.G. Meng, T. Hu, A novel route for synthesis and growth formation of metal oxides microspheres: Insights from V_2O_3 microspheres, Mater. Chem. Phys. 177 (2016) 543-553.

[42] L. Zhong, M. Li, H. Wang, Y.Y. Luo, J. Pan, G. Li, Star-shaped VO_2 (M) nanoparticle films with high thermochromic performance, Crystengcomm 17 (2015) 5614-5619.

[43] R.L. Penn, J.F. Banfield, Imperfect oriented attachment: dislocation generation in defect-free nanocrystals, Science 281 (1998) 969-971.

[44] T.D. Hedman, M.L. Gross, On the thermal stability of partially decomposed ammonium perchlorate, Propellants Explos. Pyrotech. 41 (2016) 254-259.

[45] S.S. Lu, X.Y. Jing, J.Y. Liu, J. Wang, Q. Liu, Y.H. Zhao, S. Jamil, M.L. Zhang, L.H. Liu, Synthesis of porous sheet-like Co_3O_4 microstructure by precipitation method and its potential applications in the thermal decomposition of ammonium perchlorate, J. Solid State Chem. 197 (2013) 345-351.

[46] H. Kumar, P.N. Tengli, V.K. Mishra, P. Tripathi, D.B. Pal, P.K. Mishra, Synthesis and catalytic activity of Cu-Cr-O-TiO_2 composites for the thermal decomposition of ammonium per-chlorate: enhanced decomposition rate of fuel for solid rocket motors, RSC Adv. 7 (2017) 12486-12495.

[47] S.G. Hosseini, R. Abazari, A facile one-step route for production of CuO, NiO, and CuO-NiO nanoparticles and comparison of their catalytic activity for ammonium perchlorate decomposition, RSC Adv. 5 (2015) 96777-96784.

[48] Y.F. Zhang, J.C. Zhang, J.R. Nie, Y.L. Zhong, X.H. Liu, C. Huang, Facile synthesis of V_2O_3/C composite and the effect of V_2O_3 and V_2O_3/C on decomposition of ammonium perchlorate, Micro.

Nano. Lett. 7(8) (2012).

[49] Z.K. Zhang, D.Z. Guo, G.M. Zhang, Preparation, characterization and catalytic property of CuO nano/microspheres via thermal decomposition of cathode-plasma generating $Cu_2(OH)_3NO_3$ nano/microspheres, J. Colloid Interface Sci. 357(1) (2011) 95-100.

[50] Y. Deng, Y.Y. Yang, L.Y. Ge, W.Z. Yang, K.N. Xie, Preparation of magnetic Ni-P amorphous alloy microspheres and their catalytic performance towards thermal decomposition of ammonium perchlorate, Appl. Surf. Sci. 425 (2017) 261-271.

[51] Y.F. Zhang, X.F. Tan, C.G. Meng, The influence of VO_2(B) nanobelts on thermal decomposition of ammonium perchlorate, Mater. Sci. 33 (2015) 560-565.

[52] Y.F. Zhang, X.H. Liu, J.R. Nie, L. Yu, Y.L. Zhong, C. Huang, Improve the catalytic activity of α-Fe_2O_3 particles in decomposition of ammonium perchlorate by coating amorphous carbon on their surface, J. Solid State Chem. 184 (2011) 387-390.

- V_2O_3 microspheres are synthesized by the supercritical solvothermal method.
- The formation mechanism is proposed based on the self-assembly process.
- The thermal decomposition temperature of AP with 2 wt% of V_2O_3 is reduced by 46 °C.
- V_2O_3 microspheres show excellent catalytic activity for the decomposition of AP.